Falloff Curves and Mechanism of the Thermal Decomposition of CF_3I in Shock Waves

C. J. Cobos[a], L. Sölter[b], E. Tellbach[b], J. Troe[b,c,*]

Electronic Supporting Information (ESI)

[a] INIFTA, Facultad de Ciencias Exactas, Universidad Nacional de La Plata, CONICET,

Casilla de Correo 16, Sucursal 4, La Plata (1900), Argentina

[b] Institut für Physikalische Chemie, Universität Göttingen, Tammannstrasse 6, D-37077 Göttingen, Germany

[c] Max-Planck-Institut für Biophysikalische Chemie, Am Fassberg 11, D-37077 Göttingen, Germany

*jtroe@gwdg.de

ESI-1 Modelling of Rate Constants

(i) Quantum-chemical calculations

With the quantum-chemical calculations described in Section II of the main article, the following results for the relevant potential energy surface (PES) of the reaction were obtained. Fig. S1 shows the minimum energy path (MEP) potential V as a function of the CF_3-I center-of-mass distance bond r. The dashed curve corresponds to a Morse potential with the Morse parameter $\beta_e = 1.45$ Å^{-1} while the full curve (at $r > 3.2$ Å) corresponds to a representation with $\beta_e = 1.64$ Å^{-1} (a simple estimate of β_e with the C-I stretching frequency $\nu = 286$ cm^{-1} and the Morse bond energy $D_e = 225.9$ kJ mol^{-1} would have led to $\beta_e = 1.69$ Å^{-1}). Besides the r-dependence, the anisotropy of the PES is of importance. It is represented by the r-dependence of the transitional mode frequencies ν shown in Fig. S2. These frequencies decay exponentially with increasing r with decay parameters $\alpha = 0.6$ (± 0.01) Å^{-1}. The ratio $\alpha / \beta_e = 0.4$ is slightly below the "standard value" of 0.5, found for simple bond fission processes [1]. This indicates a comparably rigid activated complex of the reaction. Of further relevance are the effective rotational constants (B+C) / 2 of the PES as a function of r, such as shown in Fig. S3. These quantities lead to the centrifugal barriers $E_0(J)$, the centrifugal partition functions Q_{cent}, as well as the rotational factors F_{rot} (entering the calculation of [2]).

(ii) Rate constants

The centrifugal partition functions Q_{cent} form an essential part of the high-pressure rate constants k_∞^{PST} in terms of phase space theory (PST) neglecting the anisotropy of the PES. Accounting for the anisotropy introduces a rigidity factor $k_\infty = f_{rigid} k_\infty^{PST}$ which is smaller than unity. It is convenient to estimate f_{rigid} from the analytical representation of classical trajectory calculations in terms of SACM/CT [3]. Table S1 shows results for f_{rigid} and k_∞ together with the corresponding recombination rate constants. These rate constants are approximated by

$$k_\infty = 5.9 \times 10^{15} (T/1000\ K)^{-2.2} exp(-28930\ K/T) s^{-1} \quad \text{(S1)}$$

$$k_{rec,\infty} = 6.7 \times 10^{12} (T/1000\ K)^{0.5} cm^3 mol^{-1} s^{-1} \quad \text{(S2)}$$

It appears worth mentioning that RRKM calculations of k_∞ from [4], with estimated transition state properties, leading to

$$k_\infty = 1.7 \times 10^{15} exp(-27900\ K/T) s^{-1} \quad \text{(S3)}$$

for 950 – 1200 K, are close to eq. (S1) (being a factor of 0.74 below the present k_∞ at 1000 K).

Low pressure rate constants k_0 are calculated following the method of [2]. Strong collision values k_0^{SC} employ rotational factors F_{rot} based on Figs. S1 and S3. Table S2 shows the results. Weak collision effects are described by the collision efficiency factors β_c which are related to the average (total) energies transferred per collision $\langle \Delta E \rangle$. Identifying $\langle \Delta E \rangle$ with the measured values of $-\langle \Delta E \rangle / hc \approx 100\ cm^{-1}$ from [5] and assuming only a weak temperature dependence of $\langle \Delta E \rangle$, one determines β_c such as included in Table S2. $k_0 = \beta_c k_0^{SC}$ then is represented by

$$k_0 = [Ar]\ 5.4\ \times 10^{21} (T/1000\ K)^{-10.5} exp(-31360\ K/T) cm^3 mol^{-1} s^{-1} \quad \text{(S4)}$$

or approximated by

$$k_0 \approx [Ar]\ 1.6\ \times 10^{16} exp(-19200\ K/T) cm^3 mol^{-1} s^{-1} \quad \text{(S5)}$$

One notes that the present k_0 (1000 K) is about a factor of 5 smaller than that of [4] although both calculations used the same formalism [2]. As similar collision efficiencies were used, the difference must have been in the rotational factors F_{rot}. The anisotropy of the PES, which follows from the quantum-chemical calculations of the present work, apparently was neglected in [4].

Besides k_0 and k_∞, the construction of the full falloff curves requires the determination of the center broadening factors F_{cent}. Strong collision values with the method of [6] were determined to be F_{cent}^{SC} = 0.27, 0.23, 0.21, and 0.23 for T / K = 750, 1000, 1500, and 2000, respectively. Weak collision effects add a factor of $F_{cent}^{WC} \approx 0.64$ [7]. With $F_{cent} = F_{cent}^{SC} F_{cent}^{WC}$, the present work employs the representation of the falloff curves from [7, 8] in the form

$$k/k_\infty = [x/(1+x)] F(x) \quad \text{(S6)}$$

where $x = k_0/k_\infty$ and

$$F(x) \approx (1+x)/(1+x^n)^{1/n} \quad \text{(S7)}$$

with $n = \left[(ln2)/ln\left(2/F_{cent}\right)\right][0.8 + 0.2x^q]$ and $q = (F_{cent} - 1)/ln(F_{cent}/10)$. The corresponding falloff curves are shown in Figs. S4 and S5 (and tabulated in Table S3). The comparison of Fig. S5 with the modelled falloff curves from [4] indicates that the described differences are relevant only outside the

range of the experimentally used bath gas concentrations. On the other hand, the present modelling of the falloff curves, without the use of empirical fit parameters, has led to satisfactory agreement with the measurements (see main text).

(iii) Molecular parameters

Vibrational frequencies (in cm^{-1})

CF_3I: 260 (2), 286, 537 (2), 742, 1080, 1187 (2) (from [9]);

CF_3: 508.7 (2), 701.4, 1086, 1253.8 (2) (from [10]).

Rotational constants (in cm^{-1})

CF_3I: 0.193, 0.0505, 0.0505 ($\sigma = 3$; from M06-2X calculations, see ESI-1 (i);

CF_3: 0.364, 0.364, 0.189 ($\sigma = 3$; from [11]).

Lennard Jones parameters: $\sigma(CF_3I) \approx \sigma(CF_3Br) = 4.92$ Å, $\varepsilon/k(CF_3I) \approx \varepsilon/k(CF_3Br) = 249$ K, $\sigma(Ar) = 3.47$ Å, ε/k (Ar) = 114 K (from [12]).

ESI-2 Modelling of Spectral Properties

For a series of species which are possibly present in the mechanism, spectral properties were calculated using time-dependent density functional theory (TD-DFT, details of the present approach are described in [13]). Here only average results for the lowest excited electronic states are reported (for nine of the models used in [13]). Results for higher states are given only for the M06-2X model. TD-DFT calculations for CF_3I used 6-311+G(3df) basis sets for C and F, as well as 6-311G(d) for I (see main text). The wavelength λ_{max} of the longest wavelength continuum was calculated to be 260 (± 6) nm in good agreement with the experimental value of 263 nm [14]. Results were λ_{max} / nm = 256, 256, 154, 154, and 154 for the five lowest excited electronic states with oscillator strengths f = 0.0020, 0.0019, 0.135, 0.137, and 0.30, respectively. Calculations for CF_2I, using the same basis sets, in the M06-2X model led to λ_{max} / nm = 367, 335, 315, 246, 240, 213, 211, and 200, with the corresponding f = 0.014, 0.0001, 0.026, 0.0006, 0.0002, 0.018, 0.006, and 0.11, respectively. Calculations for CFI led to λ_{max} / nm = 575, 334, 294, 237, 224, and 200, with f = 0.001, 0.0000, 0.0005, 0.05, 0.007, and 0.44. Calculations for FI led to λ_{max} / nm = 425, 425, 171, and 171 with f = 0.0009, 0.0009, 0.008, and 0.008. Calculations for I_2 with the same model gave λ_{max} / nm = 530, 530, 301, 301, and 184 with the corresponding f = 0.0004, 0.0004, 0.0000, 0.0000, and 1.15. Results for CF_2 and CF were found to be consistent with the calculations from [13]. E. g., in ωB97X-D calculations, λ_{max} = 256 nm with f = 0.035 was obtained for CF_2, whereas λ_{max} = 303, 222, and 197 nm with f = 0.007, 0.026, and 0.048 was obtained for CF. A comparison of the results for I_2 and FI obviously is most relevant for the tentative assignment of the spectrum near 450 and 200 nm to I_2 as well as FI, see main text.

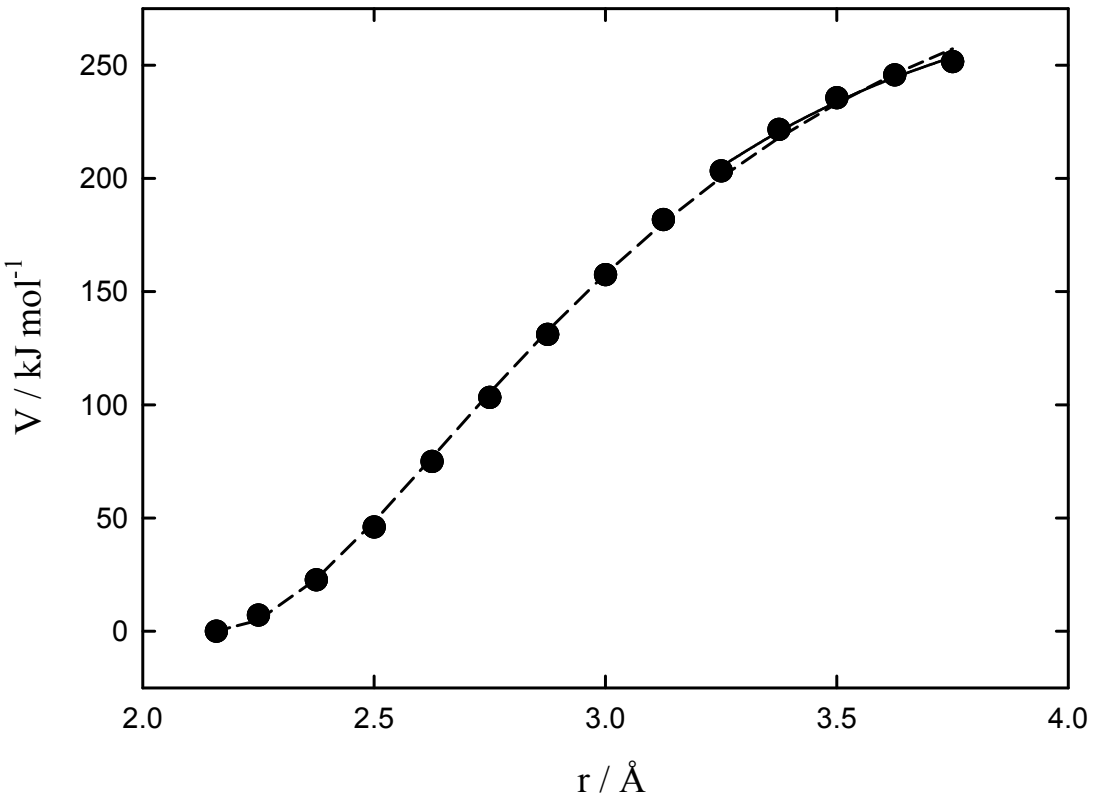

Figure S1. Electronic potential for the $CF_3I \rightarrow CF_3 + I$ reaction calculated at the CCSD(T)//M06-2X level (see text).

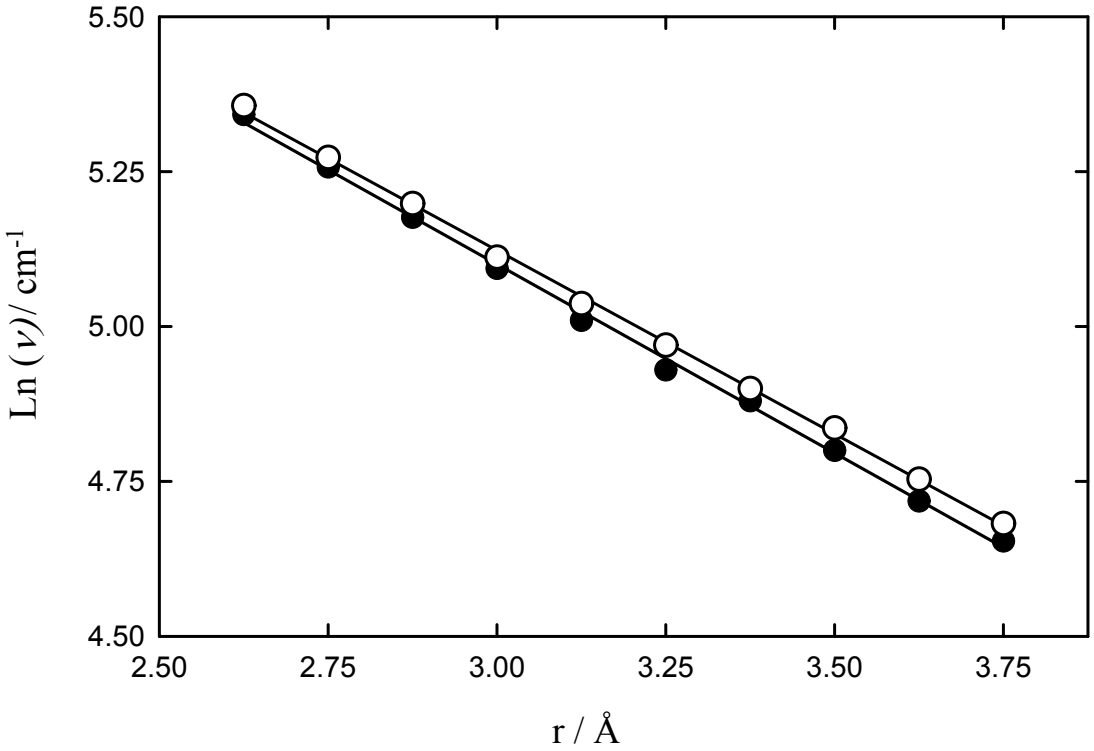

Figure S2. Torsional transitional modes of CF_3I calculated at the M06-2X level along the MEP (see text).

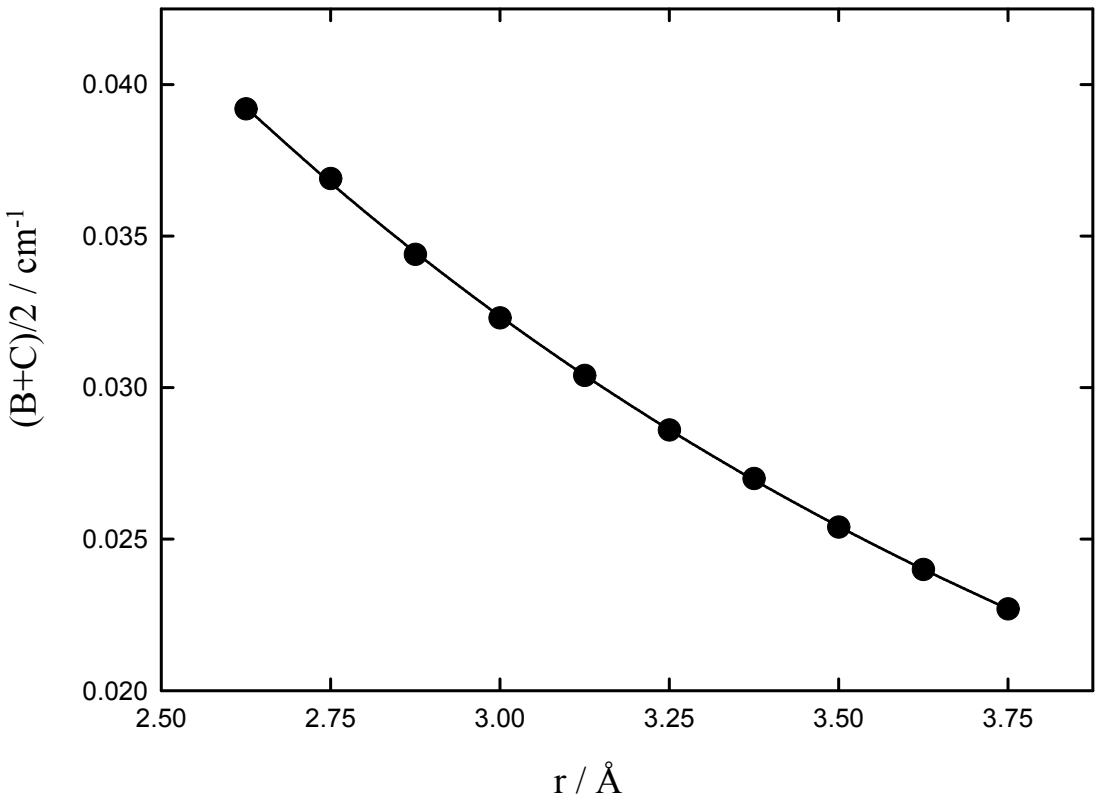

Figure S3. Rotational constants of CF_3I calculated at the M06-2X level along the MEP (see text).

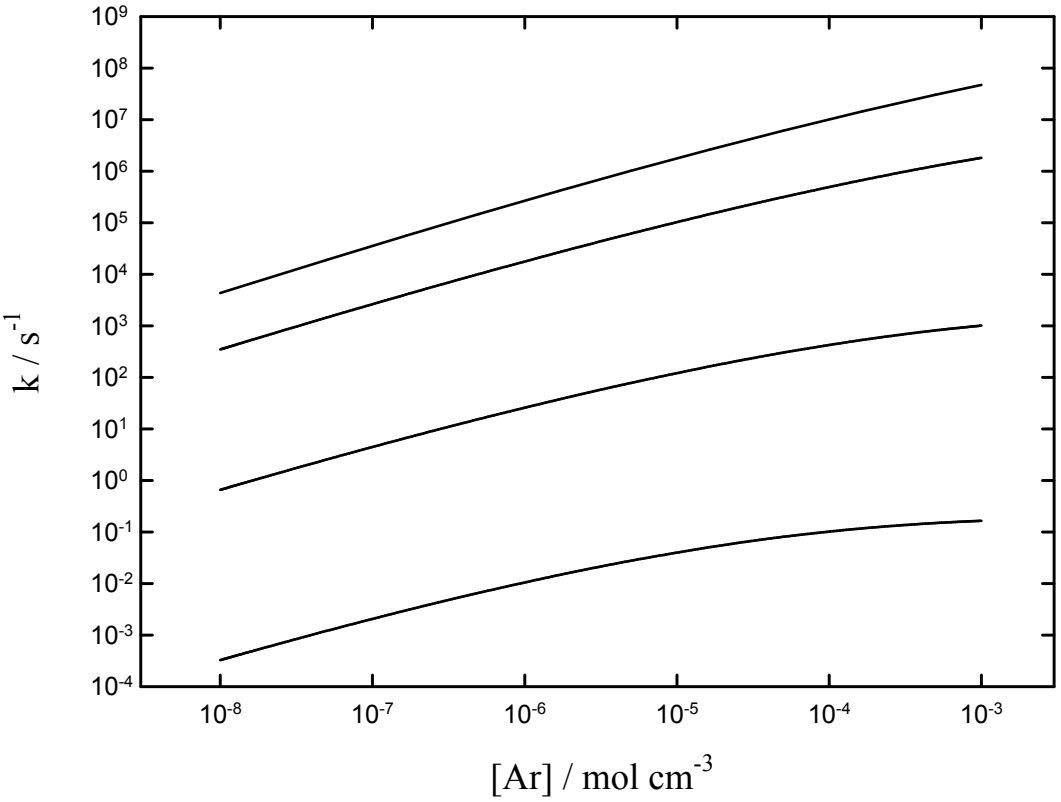

Figure S4. Modelled falloff curves for $CF_3I + Ar \rightarrow CF_3 + I + Ar$. Calculations for 750, 1000, 1500 and 2000 K (from bottom to top).

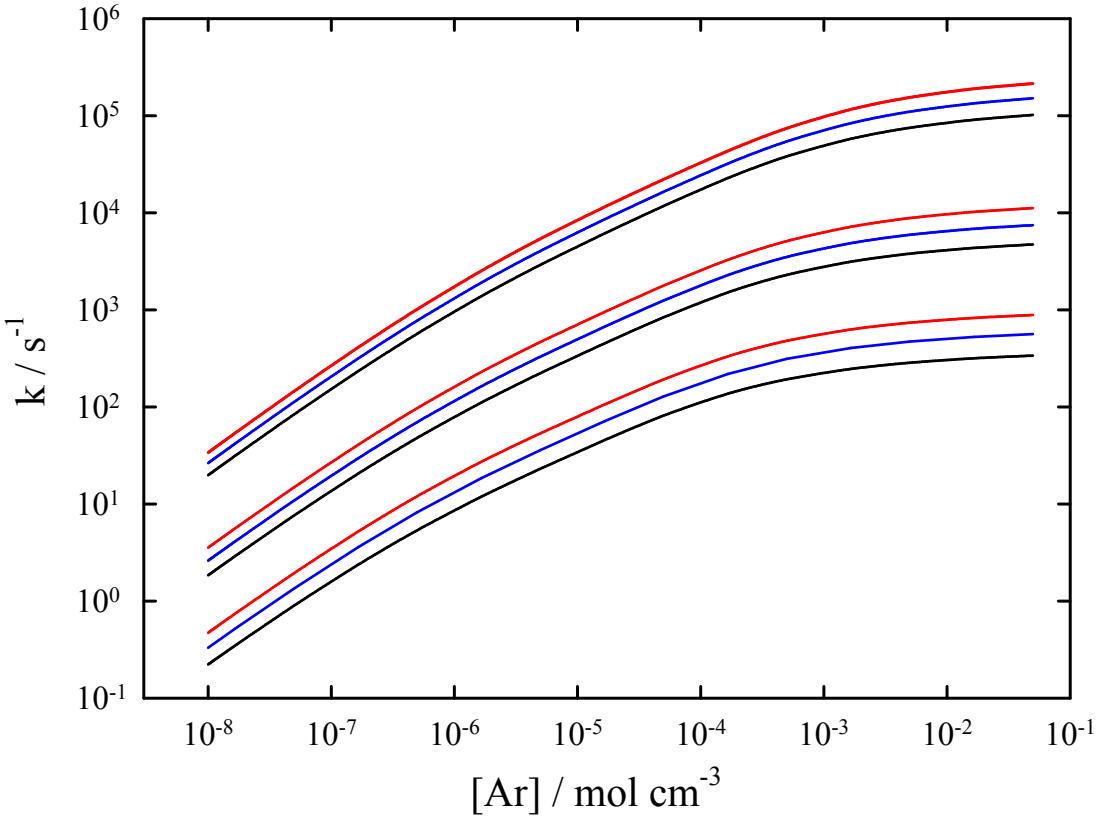

Figure S5. Modelled falloff curves for $CF_3I + Ar \rightarrow CF_3 + I + Ar$. Calculations for 950, 1050 and 1200 K (from bottom to top). Black: calculated with ΔH°_0= 224.7 kJ mol^{-1}. Blue: calculated with ΔH_0^0 = 220.5 kJ mol^{-1}. Red: calculated with ΔH°_0= 216.7 kJ mol^{-1}.

T / K	k_∞	f_{rigid}	$k_{rec,\infty}^{PST}$	$k_{rec,\infty}$
750	1.98 × 10^{-1}	9.96 × 10^{-2}	5.81 × 10^{13}	5.78 × 10^{12}
1000	1.62 × 10^{5}	1.07 × 10^{-1}	6.26 × 10^{13}	6.75 × 10^{12}
1500	1.03 × 10^{7}	1.19 × 10^{-1}	6.99 × 10^{13}	8.31 × 10^{12}
2000	6.76 × 10^{8}	1.28 × 10^{-1}	7.53 × 10^{13}	9.64 × 10^{12}

Table S1 Calculated limiting high-pressure dissociation rate constants k_∞ (in s^{-1}) for $CF_3I \rightarrow CF_3 + I$ with $\Delta H_0^\circ = 224.7\ kJ\ mol^{-1}$, rigidity factors $f_{rigid} = k_\infty/k_\infty^{PST} = k_{rec,\infty}/k_{rec,\infty}^{PST}$, and recombination rate constants $k_{rec,\infty}$ (in $cm^3\ mol^{-1}\ s^{-1}$) for $CF_3 + I \rightarrow CF_3I$ (see text).

T / K	k_0^{SC} / [Ar]	β_c	k_0 / [Ar]
750	7.03 × 10^{5}	0.106	7.45 × 10^{4}
1000	1.80 × 10^{9}	0.078	1.40 × 10^{8}
1500	1.26 × 10^{12}	0.048	6.04 × 10^{10}
2000	1.93 × 10^{13}	0.032	6.19 × 10^{12}

Table S2 Calculated limiting low-pressure rate constants k_0 / [Ar] (in $cm^3\ mol^{-1}\ s^{-1}$) for $CF_3I + Ar \rightarrow CF_3 + I + Ar$ (with $\Delta H_0^\circ = 224.7\ kJ\ mol^{-1}$) ($k_0^{SC}$ = strong collision rate constants, $\beta_c = k_0/k_0^{SC}$ = collision efficiencies calculated with $\langle \Delta E \rangle / hc = -100\ cm^{-1}$; see text).

[Ar] / mol cm^{-3}	k (950 K)	k (1050 K)	k (1200 K)
1.66 × 10^{-6}	1.19 × 10^{1}	1.11 × 10^{2}	1.39 × 10^{3}
4.98 × 10^{-6}	2.30 × 10^{1}	2.22 × 10^{2}	2.90 × 10^{3}
1.66 × 10^{-5}	4.55 × 10^{1}	2.45 × 10^{2}	6.13 × 10^{3}
4.98 × 10^{-5}	8.13 × 10^{1}	8.35 × 10^{2}	1.17 × 10^{4}
1.66 × 10^{-4}	1.37 × 10^{2}	1.51 × 10^{3}	2.28 × 10^{4}
4.98 × 10^{-4}	1.92 × 10^{2}	2.29 × 10^{3}	3.80 × 10^{4}
1.66 × 10^{-3}	2.46 × 10^{2}	3.35 × 10^{3}	5.78 × 10^{4}

Table S3 Calculated rate constants k (in s^{-1}) for $CF_3I + Ar \rightarrow CF_3 + I + Ar$ (with $\Delta H_0^\circ = 224.7\ kJ\ mol^{-1}$, see text).

References

(1) Cobos, C. J.; Troe, J. Theory of Thermal Unimolecular Reactions at High Pressures. II. Analysis of Experimental Results. *J. Chem. Phys*. 1985, **83**, 1010-1015.

(2) J. Troe, Predictive Possibilities of Unimolecular Rate Theory, *J. Phys. Chem.* 1979, **83**, 114 – 126.

(3) A. I. Maergoiz, E. E. Nikitin, J. Troe, V. G. Ushakov, Classical Trajectory and Statistical Adiabatic Channel Study of the Dynamics of Capture and Unimolecular Bond Fission. V. Valence Interactions between Linear Rotors. *J. Chem. Phys*. 1998, **108**, 9987 – 9998.

(4) N. S. Bystrov, A. V. Emelianov, A. V. Eremin, P. I. Yatsenko, Direct Measurements of Rate Coefficients for Thermal Decomposition of CF_3I using Shock-Tube ARAS technique, *J. Phys. D: Appl. Phys.* 2018, **51**, 1 – 8.

(5) B. Abel, H. Hippler, J. Troe, Infrared Multiphoton Excitation Dynamics of CF_3I. II. Collisional Effects on Vibrational and Rotational State Populations, *J. Chem. Phys.* 1992, **96**, 8872 – 8876.

(6) J. Troe, Theory of Thermal Unimolecular Reactions in the Falloff Range. I. Strong Collision Rate Constants. *Ber. Bunsenges. Phys. Chem*. 1983, **87**, 161 – 169.

(7) J. Troe, V. G. Ushakov, Revisiting Falloff Curves of Thermal Unimolecular Reactions. *J. Chem. Phys.* **2011**, 135, 054304.

(8) J. Troe, V. G. Ushakov, Representation of "Broad" Falloff Curves for Dissociation and Recombination Reactions. *Z. Phys. Chem.* 2014, **228**, 1 – 10.

(9) T. Shimanouchi, Tables of Molecular Vibrational Frequencies, Consolidated Volume II*, J. Phys. Chem. Ref. Data* 1972, **6**, 993-1102.

(10) D. Forney, M. E. Jacox, K. K. Irikura, Matrix-Isolation Study of the Interaction of Excited Neon Atoms with CF_4.Infrared Spectra of CF_3^+ and CF_3^-. *J. Chem. Phys.* 1994 **101**, 8290 - 8296.

(11) C. Yamada, E. Hirota, Infrared Diode Laser Spectroscopy of the CF_3 ν_3 Band. *J. Chem. Phys.* 1983, **78**, 1703 - 1711.

(12) H. Hippler, J. Troe, H. J. Wendelken, Collisional Deactivation of Highly Excited Polyatomic Molecules. 2. Direct Observation for Excited Toluene. *J. Chem. Phys.* 1983, **78**, 6709 - 6717.

(13) Cobos, C. J.; Knight, G.; Sölter, L.; Tellbach, E.; Troe, J. Kinetic and Spectroscopic Studies of the Reaction of CF_2 with H_2 in Shock Waves. *J. Phys. Chem. A* 2017, **121**, 7827 – 7834.

(14) B. Abel, B. Herzog, H. Hippler, J. Troe, Infrared Multiphoton Excitation of CF_3I. II. Collisional Energy Transfer of Vibrationally Highly Excited CF_3I, *J. Chem. Phys.* 1989, **91**, 900 – 905.